iScience

CellPress
OPEN ACCESS

Article

Tunable circular conversion dichroism of single-layer twisted graphene-patterned metasurface

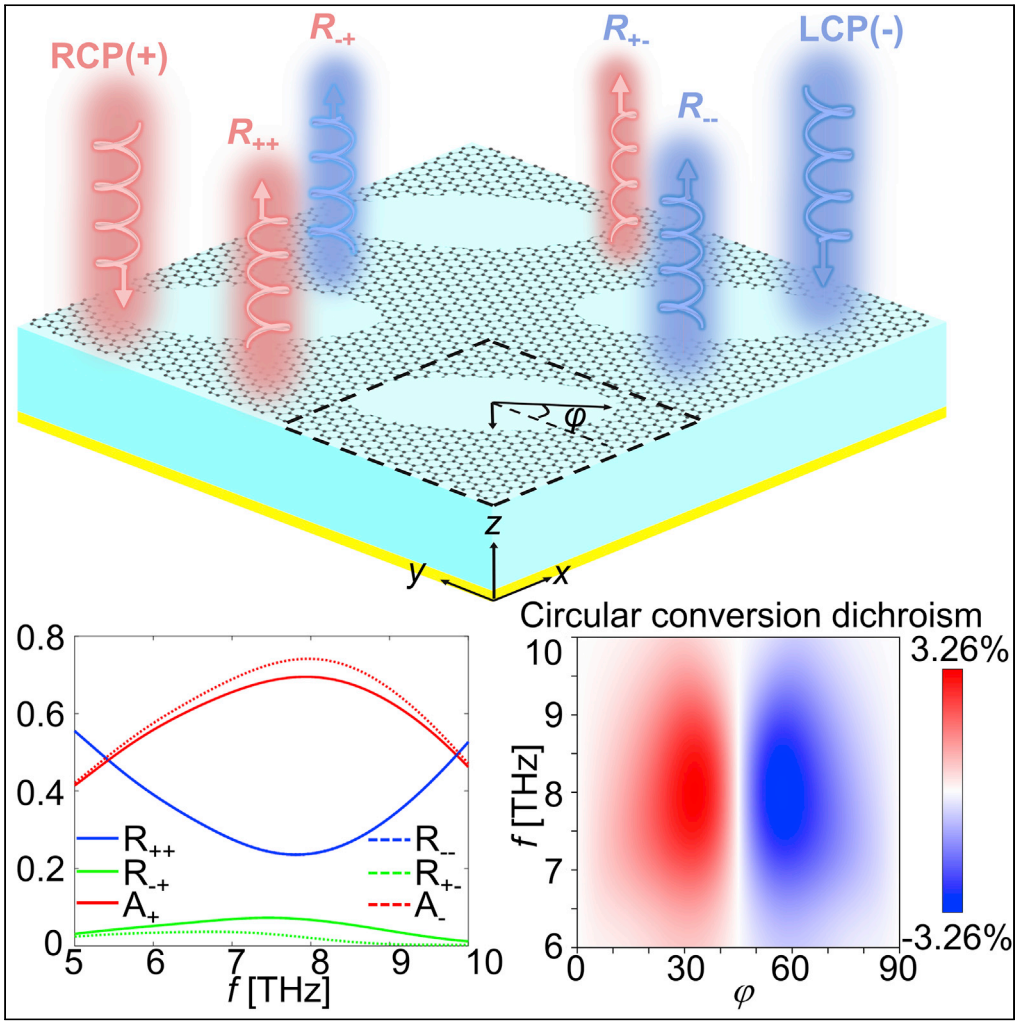

Yali Zeng, Qilin Duan, Jinying Xu, Zhilin Yang, Huanyang Chen, Yineng Liu

kenyon@xmu.edu.cn (H.C.)
lyn610@xmu.edu.cn (Y.L.)

Highlights

Intrinsic structural 2D-chirality can be generated in achiral unit cell arrays

Graphene metasurface is proposed to achieve THz dynamically tunable CCD

Multiband enhanced CCD is realized in the graphene metasurface

Zeng et al., iScience 26, 106115
March 17, 2023
https://doi.org/10.1016/j.isci.2023.106115

iScience

CellPress
OPEN ACCESS

Article

Tunable circular conversion dichroism of single-layer twisted graphene-patterned metasurface

Yali Zeng,[1] Qilin Duan,[1] Jinying Xu,[2] Zhilin Yang,[1] Huanyang Chen,[1,*] and Yineng Liu[1,3,*]

SUMMARY

Two-dimensional (2D) chirality-induced asymmetric transmission/reflection has great potential for polarization applications. Usually, asymmetric effects resulting from circular conversion dichroism (CCD) occur in chiral metasurfaces. Here, we propose a single-layer twisted graphene-patterned (with tilted elliptical hole arrays) metasurface and theoretically reveal its tunable CCD in the terahertz (THz) region. The unit cell of the metasurface is achiral. Merely by altering the in-plane orientation of holes for structural 2D chirality, a tunable CCD can be achieved at normal incidence. Interestingly, the reflection phase can be considered an intuitive method to show this metasurface's anisotropy, which complements the conventional CCD measurement in characterizing chiral materials. Furthermore, we can achieve active CCD based on the tunability of graphene. Due to the Fabry-Pérot resonance, a multiband enhancement of CCD spectrum will happen by changing the dielectric layer thickness. The proposed metasurface provides more flexible opportunities for designing active THz devices for polarization manipulation.

INTRODUCTION

Chiral objects exhibit different responses when interacting with circularly polarized waves (CPW) with opposite handedness. The definition of chirality is first defined in three dimensions (3D).[1] Similar to 3D chirality, the definition of chirality can also be applied in two dimensions (2D). 2D chirality can be found in planar chiral systems.[2] In contrast to 3D chiral structures, 2D planar chiral systems possess the reversed sense of twist for observation from the opposite direction. Consequently, planar chiral materials can induce different phenomena when the CPW interacts with the front and back of a lossy anisotropic planar chiral interface or the CPW with opposite handedness illuminates on a lossy anisotropic planar chiral structure, such as asymmetric transmission, reflection, and absorption.[3–12] These asymmetric effects of CPW result from the circular conversion dichroism (CCD). Those intriguing phenomena have attracted significant interest for promising applications in polarization devices such as circular polarizers, polarization rotators, and chiral detectors.

The boom in metamaterials provides a rich platform for studying chiral responses in planar chiral structures. Various artificial structured materials have been extensively explored to enhance chiral response. Particularly, metallic nanostructures and 2D material metasurfaces[3–19] are generally employed to enhance or achieve tunable chiral responses. It is reported that CCD can be observed in a lossy anisotropic chiral "fish-scale" planar structure under normal incidence of CPW.[20] Also, tunable circular polarization conversion and asymmetric transmission from 0.049% to 3.504% can be tuned by changing Fermi level in bilayer graphene-based planar chiral metamaterial in the terahertz (THz) region.[19] A chiral metasurface composed of graphene split ring arrays has been proposed to realize tunable asymmetric transmission and CCD (= 0.36).[21] These studies have focused on the metasurfaces consisting of chiral metamolecules; what about the achiral metamolecules? It is known that planar chiral structures can generate intrinsic chiral responses under normal incidence of CPW. Significantly, intrinsic structural 2D chirality also occurs in periodic arrays assembled by achiral unit cells under normal incidence of CPW, when the lines of mirror symmetry of the metamolecule in each unit cell and the mirror lines associated with the array's lattice do not coincide.[22] For example, 2D chiral phenomenon (asymmetric transmission) can be observed in arrangements of achiral asymmetrically split rings.[22] A tilted rectangular hole array in a square lattice has also been used to realize

[1]Department of Physics and Institute of Electromagnetics and Acoustics, Xiamen University, Xiamen 361005, China

[2]Department of Physics, Fuzhou University, Fuzhou 350108, China

[3]Lead contact

*Correspondence: kenyon@xmu.edu.cn (H.C.), lyn610@xmu.edu.cn (Y.L.)

https://doi.org/10.1016/j.isci.2023.106115

the asymmetric transmission effect in visible wavelengths.[23] Similarly, lattice-plasmon-induced asymmetric transmission can be achieved in a planar array of achiral tetramer nanostructures.[24] However, the aforementioned studies about intrinsic structural 2D chirality focus on metallic systems, which usually work in visible-infrared regions, and suffer from nontunable characteristics after fabrication. In addition, previously, 2D chiral response such as CCD and asymmetric reflection has rarely been discussed in the THz region, resulting in the lack of planar chiral polarization components and devices in the THz realm. Therefore, structural 2D chiral and tunable metasurfaces are also highly desirable in the THz realm to fill the "THz gap." As an ultrathin 2D material, graphene possesses excellent optical properties and very flexible tunability, and the conductivity of graphene can be changed by tuning the Fermi level via chemical or electrostatic doping. Moreover, the plasma frequency of graphene can work in the mid-infrared and THz region, which makes graphene-based THz metasurface[25–28] attractive in designing active polarization conversion, asymmetric transmission manipulation, and enhanced chirality detection. Therefore, active tuning of structural 2D chiral response in the THz region is highly worth exploring in a graphene-based metasurface.

In this work, we propose a simple graphene-based metasurface and study the CCD response under normal incidence of CPW in the THz region. The metasurface consists of a monolayer graphene pattern (etched tilted elliptical hole arrays with respect to the lattice vectors) placed on a dielectric layer with a metal substrate, which is a 2D anisotropic system. Notably, the unit cell of the graphene-based metasurface is achiral, but an intrinsic structural 2D chirality can be generated in the periodically twisted achiral unit cell arrays. At normal incidence, CCD can occur in lossy anisotropic chiral planar metasurface, and anisotropy can also induce various phase differences for reflected converted waves of CPW with opposite handedness. We observe that a tunable CCD in the THz region can be achieved in the anisotropic-structured graphene metasurface by simply altering the in-plane rotation angle of the elliptical hole in each unit cell, and inverse CCD will occur when two rotation angles are complementary. Tunable CCD can also be further enhanced by the excitation of graphene surface plasmon polaritons (SPPs). Furthermore, our proposed graphene-based metasurface is dynamically tunable by tuning the Fermi level of graphene. Because of the FP resonance between graphene and metal substrate, a multiband enhanced CCD spectrum is achieved in the THz band by adjusting the dielectric layer thickness. This work holds great promise for active polarization manipulation, biosensors, and chiral detection in the THz realm.

RESULTS AND DISCUSSION

Proposed graphene-based metasurface

Figure 1A shows the schematic diagram of the graphene-based metasurface in this work. The top layer is a monolayer graphene with twisted elliptical hole array, having major axis r_y and minor axis r_x. The second layer is a dielectric spacer and the bottom layer is a silver substrate to prevent the transmission of light. Significantly, the unit cell (black dashed box in Figure 1A) of the graphene-based metasurface is achiral, whereas the periodic metasurface forms a structural 2D chiral array for the angles φ ($\varphi \neq n \times 45^\circ$, $n \in Z$) denoting the angle between the major axis of the elliptical hole and the y axis. When the right circularly polarized (RCP) or left circularly polarized (LCP) waves illuminate into the graphene-based reflective metasurface, the reflection and absorption are different for each case, leading to 2D chiral response. It is known that the complex reflection matrix (r_{ij}, the first subscript represents the reflected wave, and the second subscript represents the incident wave), connecting the reflected wave E_i^r and the incident wave E_j^{inc} by the formula of $E_i^r = r_{ij}E_j^{inc}$, can be employed to analyze the reflection property of the metasurface. The reflection (R_{ij}) of the metasurface can also be calculated by the complex reflection matrix: $R_{ij} = |r_{ij}|^2$, 'i' and 'j' denote RCP (+) or LCP (−) wave. It is worth noting that, usually, the rotational direction of CPW will be changed in the reflection direction when the observation plane is fixed. However, in our case, the handedness of the incident and reflected CPW is determined by the corresponding wave vector, respectively. RCP wave and LCP wave mean the electric field vectors of the waves rotate clockwise and counterclockwise when viewed along the wave vector direction/propagation direction, respectively. The observation plane of the incident and reflected CPW are not identical in our definition. Consequently, the 2D chiral response CCD can be obtained by: $CCD = R_{-+} - R_{+-} = |r_{-+}|^2 - |r_{+-}|^2$, where R_{-+} and R_{+-} represent the conversion reflections of RCP-to-LCP wave and LCP-to-RCP wave, respectively.

The efficiency of conversion reflection has a close relationship with graphene's surface plasmon resonances. Hence, to enhance the 2D chiral response in the THz region, we calculate the CCD spectra of graphene-based metasurface with different lattice sizes by using full wave simulations with 3D finite element software (COMSOL Multiphysics), as shown in Figures 1B and 1C. The optical conductivity of graphene can

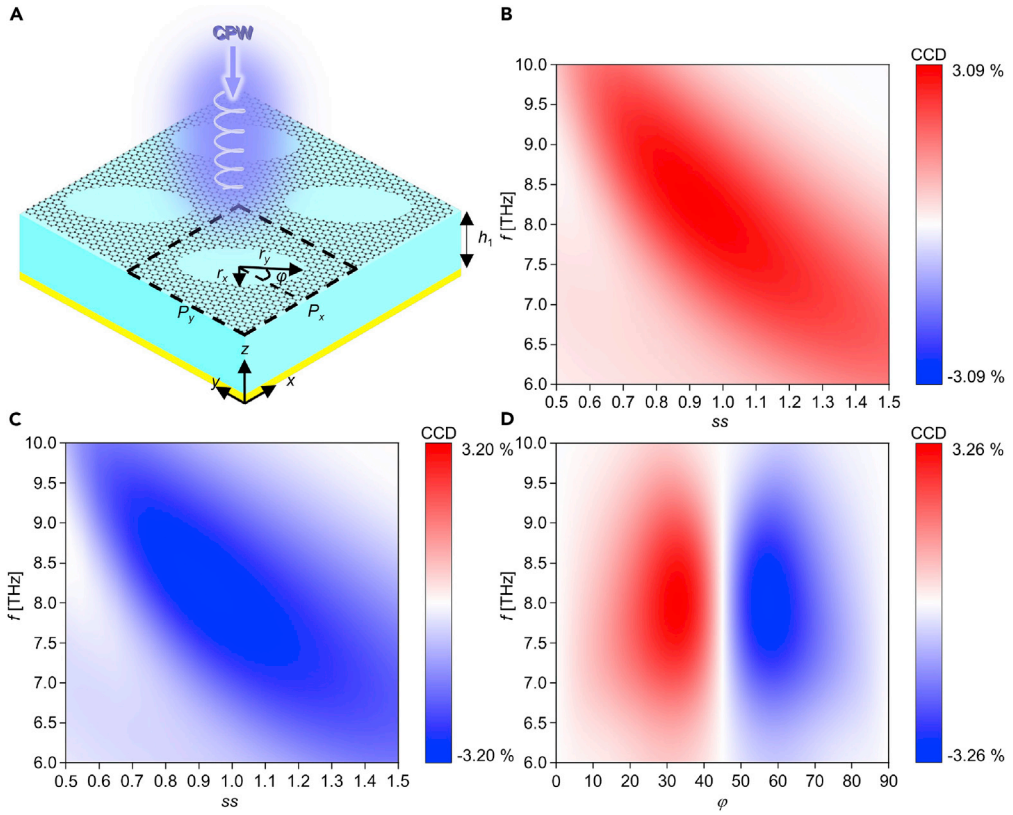

Figure 1. The intrinsic structural chirality induced by the metasurface with single-layer twisted graphene pattern

(A–C) The schematic diagram (A) of the graphene-based metasurface under normal incidence of circularly polarized wave. The CCD spectra of the proposed structure with a fixed rotation angle (B) φ = 36° and (C) φ = 60°. φ denotes the angle between the major axis of the elliptical hole and the *y* axis. *ss* denotes the scaling of the lattice period ($P = P_x = P_y$) and the major (r_y) and minor (r_x) axes of the ellipse, and the geometrical parameters are given as $P_x = P_y = 9.2\ s$ μm, $r_x = 2.5\ s$ μm, $r_y = 4.5\ s$ μm, $h_1 = 6.8$ μm.

(D) The CCD spectrum of the proposed structure with the varying rotation angle φ. The dimensional scaling *ss* is set to 1.

be described by Kubo formula,[19] and the relaxation time and Fermi level of graphene are 0.64 ps and 0.9 eV, respectively. The dielectric layer is set to be a lossless polyethylene cyclic olefin copolymer with a permittivity of 2.35. The metal substrate is modeled as a dispersive silver using Drude model: $\varepsilon_m = \varepsilon_\infty - \omega_p^2/(\omega^2 + i\omega\gamma)$. Here, ω is the angular frequency, $\omega_p = 1.39 \times 10^{16}$ rad/s is the plasma frequency, $\gamma = 2.7 \times 10^{13}$ rad/s is the scattering rate, and $\varepsilon_\infty = 3.4$ is the high-frequency constant. Firstly, without loss of generality, we set φ = 36° and keep the metasurface the same shape and scale its size to compute the CCD spectrum (Figure 1B), where *ss* denotes the scale of the lattice period ($P = P_x = P_y$) and the major (r_y) and minor (r_x) axes of the ellipse. The CCD varies obviously with size scaling, and the apparent resonance enhancement of CCD spectra can be found in the THz region. The resonances originate from the graphene SPPs. Therefore, we can achieve enhanced chiral response in the THz region by selecting an appropriate lattice size for the excitation of graphene's surface plasmon resonances. More interestingly, the resonances for CCD spectra in the THz region remain but the sign of the CCD reverses when the angle φ changes from 36° to 60°, as illustrated in Figure 1C. The change of twisted angle of the elliptical hole array can significantly affect the 2D chiral response for the proposed metasurface. What happens to the CCD spectra when the twisted angle φ changes continuously? What is the rotation angle of the positive and negative spectral phase transition of CCD?

In order to further explore this effect of the orientation of the elliptical hole on the chiral response, the CCD spectra of the graphene-based metasurface with the varying rotation angle φ are computed and plotted in Figure 1D. The 2D chiral response (CCD) is absent for the rotation angles φ = 0°, 45°, and 90°. In other words, these are also the positive and negative phase transition angles of the CCD spectrum. Because

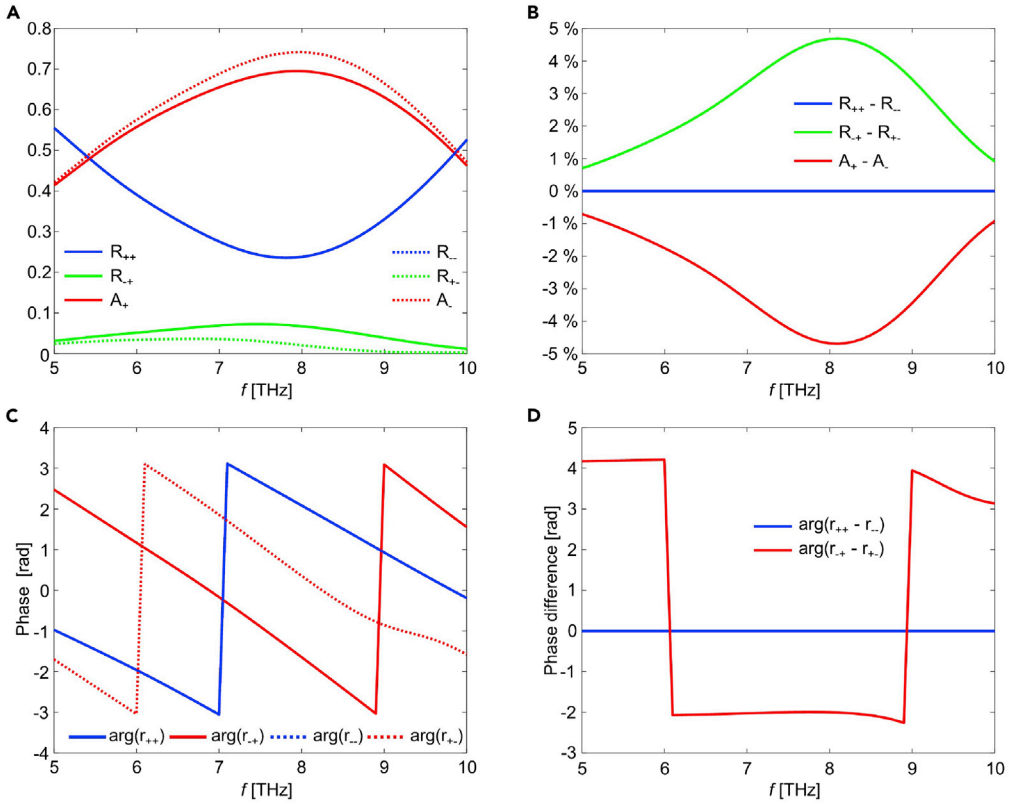

Figure 2. The 2D chiral responses for the graphene-based metasurface under normal incidence of circularly polarized wave

(A–D) The absorption and reflection spectra (A) and the absorption differences and reflection differences spectra (B) of the metasurface. The phases of reflection coefficient (C) and the phase differences of reflection coefficient (D) for the metasurface. The geometrical parameters are as follows: $\varphi = 36°$, $P_x = P_y = 8.37$ μm, $r_x = 2$ μm, $r_y = 4.85$ μm, $h_1 = 6.8$ μm. The subscripts '+' and '−' denote RCP and LCP waves, respectively.

the intrinsic structural 2D chirality derives from the orientations of the achiral metamolecules of the graphene-based metasurface, the structural 2D chirality disappears when the mirror lines of the elliptical holes coincide with those of the periodic square lattice, leading to the absence of CCD. Moreover, the CCD is positive when the rotation angle is less than 45° and negative when the rotation angle is larger than 45°. The CCD has the same value and the opposite sign when two rotation angles are complementary, which can be explained by structural symmetry. Because $\varphi = 45°$ lies on the symmetric line of the square lattice, the rotation angle φ and $(90° - \varphi)$ correspond to the structural planar chirality of opposite handedness, bringing about the inverse CCD. The results indicate that the in-plane rotation angle of individual elliptical holes in each unit cell has a vital influence on the generation of chiral response for the graphene-based metasurface. We can achieve a tunable CCD by altering the in-plane orientations of the elliptical holes.

Quantificational analyses of the chiral response

To quantificationally analyze the chiral response of the graphene-based metasurface, we draw all the absorption and reflection spectral components of the metasurface for RCP and LCP waves in Figure 2A. The absorption spectra show a resonance region around 8 THz where the absorptions of RCP and LCP waves (A_+ and A_-) are evidently different from each other. Furthermore, the reflections of right-to-right (R_{++}) waves and left-to-left (R_{--}) waves are equal, which demonstrates the absence of optical activity ($R_{++} - R_{--}$) in our structure. However, the conversion reflection for RCP (R_{-+}) wave visibly differs from that of LCP (R_{+-}) wave, indicating the dichroic response of metasurface. The corresponding reflection differences (blue and green curves) and absorption differences (red curve) spectra are depicted in Figure 2B. The CCD ($= R_{-+} - R_{+-}$ or $= A_- - A_+$) can achieve 4.68% at 8.1 THz. Considering the thickness of monolayer graphene, the circular polarization conversion efficiency here is comparable to or greater than in previously reported

Table 1. Comparison of proposed metasurface with existing typical designs

Reference	Materials used and design/ metamolecule	Frequency	Tunability	Functionality	Maximum AR/AT/CCD[a]
Huang et al., 2017[19]	Bilayer chiral S-shaped graphene pattern	Terahertz	Yes	Dual-band CCD and AT	AT∼3.504%
Asgari and Rahmanzadeh, 2020[21]	Chiral graphene split ring	Terahertz	Yes	Single-band CCD and AT	CCD∼36%
Li et al., 2020[31]	Hole in graphene layer and double layer C-shaped gold split ring	Terahertz	Yes	Single-band CD	CD∼61%
Shen and He, 2021[32]	Three layers of rotated gold split-rings	Near-infrared and mid-infrared	No	Dual-band AR and AT	AT&AR∼60%
Rana et al., 2020[33]	Four hydrogenated amorphous silicon nanofins	Visible	No	Broad band CCD and AT	CCD∼55%, AT∼58%
Fedotov et al., 2006[20]	Achiral asymmetrically split ring in copper layer	Gigahertz	No	Single-band AT	AT∼5 dB
Aba et al., 2018[23]	Achiral rectangular nanohole in gold film	Visible	No	Dual-band AT	AT∼15%
Apurv Chaitanya et al., 2022[24]	Achiral gold tetramers	Visible and near-infrared	No	Dual-band AT	AT∼36%
Our work	Achiral elliptical holes in graphene layer	Terahertz	Yes	Multiband CCD and AR	CCD&AT∼4.8%

[a]Note: AR, asymmetric reflection; AT, asymmetric transmission; CCD, circular conversion dichroism, CD, circular dichroism.

metallic metamaterials.[23,24,29,30] The measurable chiral response origins from the twist of single-layer graphene pattern and is enhanced by the graphene SPPs. Compared with the bilayer chiral graphene metasurface with 3.504% asymmetric transmission in Ref. 19, our structure requires only an ultrathin and simple single-layer graphene pattern and can achieve a higher chiral response (4.68% CCD). Purely by rotating the elliptical hole arrays, we can attain a tunable and measurable chiral response. Furthermore, more comparisons of our work with the relative references are given in Table 1. Our work provides a very simple structure to achieve tunable multiband CCD response and asymmetric reflection in the THz region.

Because of the elliptical holes in graphene, our structure is an anisotropic system that possesses different modes along the two orthogonal lattice vectors. Therefore, the changes of phases for the converted reflected waves are significantly different when the CPW with opposite handedness interacts with the anisotropic graphene-based metasurface, as shown in Figure 2C. Therefore, we can consider the reflection phase as an intuitive method to complement the conventional CCD measurement in the characterization of chiral materials.[34,35] Indeed, the spectra in Figure 2A show that the graphene-based metasurface is a highly absorbing structure, especially at the resonance frequency, and the conversion reflection is relatively small. Consequently, to clearly show this metasurface's anisotropic chirality, we draw the phases of reflection coefficients in Figure 2C. The phase of the direct reflection coefficients ($\arg(r_{++})$) of RCP wave coincides with that of LCP wave ($\arg(r_{--})$), whereas the phases of converted reflection coefficients of RCP and LCP waves are remarkably different (red solid curve and red dashed curve in Figure 2C). The corresponding phase differences between directed and converted polarization components are drawn in Figure 2D. The obvious phase differences of converted reflection coefficients result from the metasurface's anisotropy, implying the different rotational capabilities of the polarized plane. The difference depends on the orientation of the meander's direction of the metasurface with respect to the mirror line,[20] which also provides another workable solution for the characterization of chiral metasurfaces.

Physical mechanism of the CCD

Next, we explore the physical mechanism of the enhanced CCD. There is an evident absorption peak around 8 THz in Figure 2A, which origins from the excitation of graphene SPPs. In addition, the efficiency of conversion reflection is also closely related to graphene surface plasmonic polariton resonances.

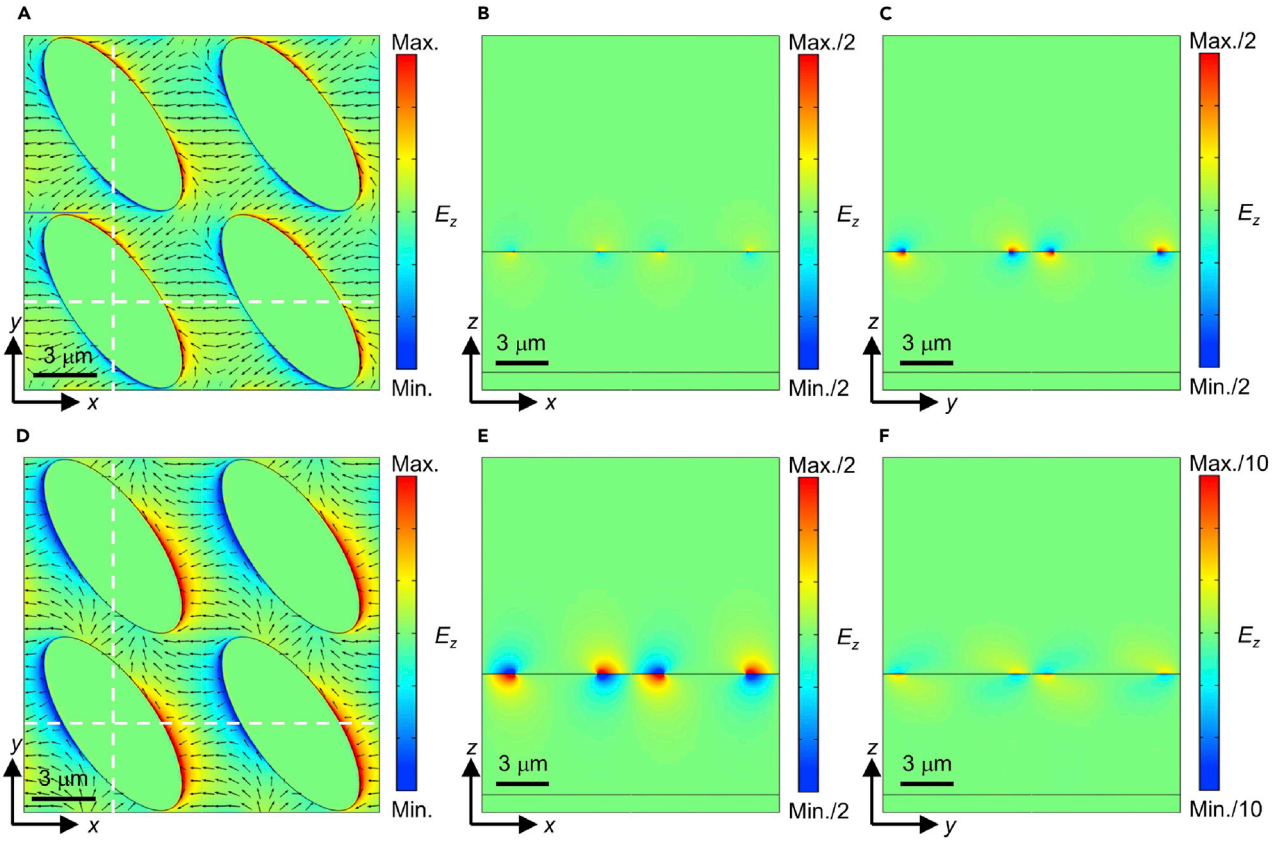

Figure 3. The electric field distributions E_z for the graphene-based metasurface (2 × 2 unit cells)

(A–F) The top view of E_z distributions under the RCP (A) and LCP (D) illuminations at f = 8.1 THz. The black arrows denote the surface current distributions. The front view E_z distributions along the horizontal white dashed lines in Figures 3A and 3D under the RCP (B) and LCP (E) illuminations at f = 8.1 THz. The side views of E_z distributions along the vertical white dashed lines in Figures 3A and 3D under the RCP (C) and LCP (F) illuminations at f = 8.1 THz.

Therefore, we show the electric field distributions and the surface current distributions (black arrows) for the graphene-based metasurface at the peak frequency of CCD (f = 8.1 THz) in Figure 3. Under RCP wave illumination, the electric field mainly concentrates around the edge of elliptical holes and distributes on both sides of the long axis of the elliptical holes (Figure 3A), manifesting the excitation of graphene SPPs. The corresponding surface currents are shown by the black arrows in Figure 3A. There are apparent surface currents flowing from right to left between horizontally adjacent elliptical holes and the surface currents flowing from top right to bottom left between vertically adjacent elliptical holes, which indicates the electric dipole moment and strong coupling between the electric field around horizontally and vertically adjacent elliptical holes. Relatively, the surface currents distributions between diagonally elliptical holes (upper left and lower right elliptical holes) are less, showing weak interaction of the electric field around the diagonal adjacent elliptical holes. The 2D chiral response induced by the single-layer twisted graphene pattern depends on the interaction between the elliptical holes in the arrays, not the individual achiral unit cell. In addition, the front and side views of the electric field along the horizontal and vertical white dashed lines in Figure 3A are depicted in Figures 3B and 3C, respectively. The clear positive and negative charge distributions around the edge represent the graphene SPPs. The graphene SPPs excited by vertically adjacent elliptical holes are close and more easily coupled to each other (Figure 3C).

The intensity of the electric field for LCP wave is stronger than that of RCP wave (Figure 3D), which demonstrates the greater absorption at the resonant frequency (Figure 2A). Furthermore, the position of electric field enhancement and the surface current distributions for LCP wave (Figure 3D) significantly differ from that of RCP wave. The electric field for LCP wave mainly distributes on half of the long axis of the elliptical holes. Moreover, except for strong surface currents distributions between horizontally and vertically

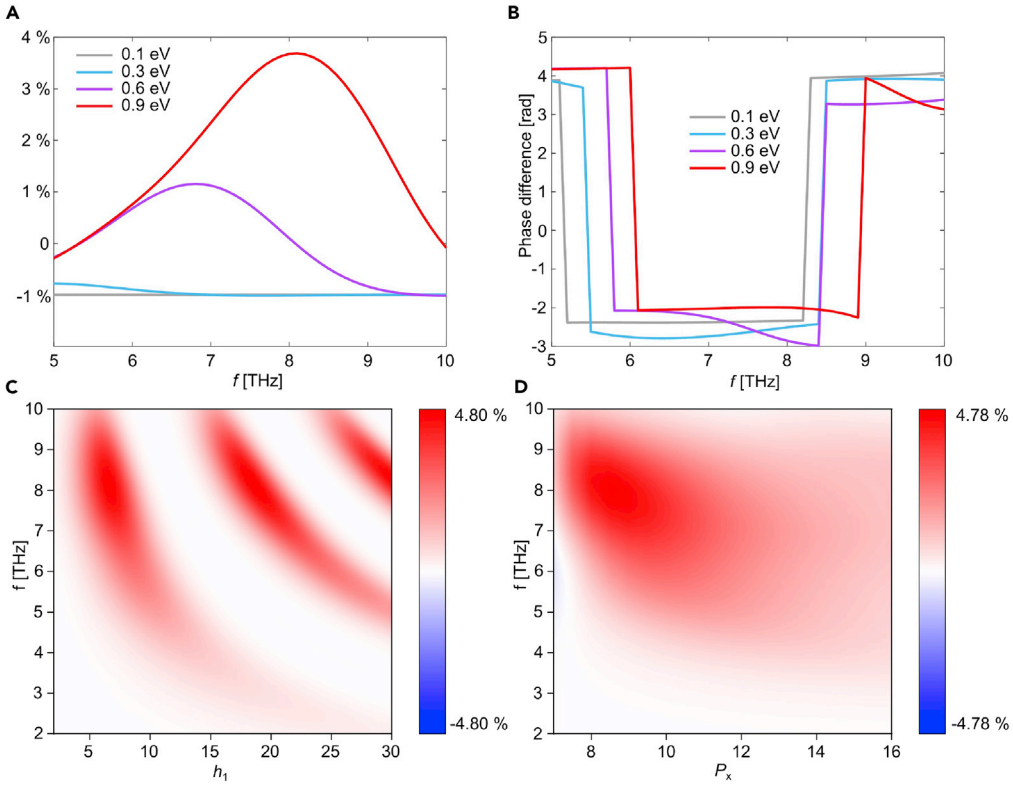

Figure 4. The tunable chiral responses of the graphene metasurface

(A and B) The CCD spectra (A) and the phase differences of reflection coefficient (B) of the metasurface with Fermi level E_F changing from 0.1 eV to 0.9 eV.

(C) The CCD spectra of the metasurface with the altered thickness of dielectric layer.

(D) The CCD spectra of the metasurface with the different lattice constants along the *x* direction.

adjacent elliptical holes, there exist nonnegligible surface currents distributions between the diagonally adjacent elliptical holes (upper left and lower right elliptical holes) under LCP wave illumination, suggesting the strong coupling between the electric field around the diagonally adjacent elliptical holes. The corresponding front and side views of the electric field for LCP wave are drawn in Figures 3E and 3F. The E_z distribution in the front view is strong, but the field in the side view is very weak. The obvious intensity differences show the extremely inhomogeneous distribution of the graphene SPPs along the long side of the elliptical holes. The different appearance of graphene SPPs is the origin of the CCD of the graphene-based metasurface.

Tunability of the CCD response

Finally, the tunability of the graphene-based metasurface has been studied. On one hand, because of the flexible switchable abilities of graphene, the CCD relating to the rotation angle can be actively tuned by the Fermi Level E_F of graphene (Figure 4A). When the Fermi Level E_F is low, the CCD is small for the weak conductivity of graphene. As the Fermi level increases, the CCD becomes large and the resonance peak also shifts to higher frequencies. Similarly, the phase difference also changes and shifts to high frequencies when we increase the Fermi level (Figure 4B), which indicates the altering of the graphene-based metasurface's anisotropy. On the other hand, except for the active adjustment methods based on graphene, the geometric parameters can also be employed to effectively tune the chiral response of the graphene-based metasurface. Because of the metal substrate, a Fabry-Pérot cavity will be generated between the graphene pattern and the metal substrate. As a consequence, we can take advantage of Fabry-Pérot resonance to adjust the chiral response. For instance, when we change the thickness of the middle dielectric, a multiband enhanced CCD will be obtained in the THz region (Figure 4C) and the CCD can be enhanced to 4.8%. Certainly, we can also get a multiband CCD spectrum by changing the refractive index of the dielectric layer. In addition, the sizes and types of lattices can also affect the value of CCD. Here, we vary the period

P_x of the metasurface (Figure 4D), and the magnitude and sign of the CCD will be altered. Both active and passive approaches can be used to adjust the 2D chiral response of our structure.

Conclusions

In summary, we have demonstrated that an active tunable and enhanced CCD in the THz region can be achieved in a single-layer twisted graphene-patterned metasurface. The CCD response arising from the rotation angle of single-layer twisted graphene pattern is enhanced by the graphene SPPs and can be dynamically tuned by the Fermi level of graphene. Moreover, we can achieve the multiband enhancement phenomenon and adjust the position and number of the resonant peak of CCD spectrum in the desired band by controlling the Fabry-Pérot resonance between graphene and metal substrate, and the CCD can be enhanced to 4.8%. Similarly, other geometric parameters of the lattice can also have a vital influence on CCD. Furthermore, graphene-based metasurface can also be combined with a metallic structure to achieve larger and tunable CCD. Therefore, our study holds great promise for the design of active THz controllable and compact polarized devices.

Limitations of the study

In this study, we propose an active graphene metasurface that can achieve a dynamically tunable and multiband enhanced CCD in the THz region, whereas we cannot conduct the device fabrications and performance measurements due to the lack of experimental conditions. Based on the previous work,[36,37] the graphene metasurface can be possibly fabricated as follows: first, a layer of silver is deposited on the bottom of polyethylene cyclic olefin copolymer (Topas) by electron beam evaporation. Next, the graphene layers were grown on copper foil by chemical vapor deposition (CVD) and then wet-transferred to Topas layers. Finally, a 100 nm layer of electron beam resist is spin coated on the chip, and the elliptical hole arrays are exposed using electron beam lithography. After resisting development, elliptical arrays are etched in oxygen plasma. Resist stripping is done in acetone, followed by IPA and DI water rinsing. In future studies, we may seek cooperation for device fabrication and measurement.

STAR★METHODS

Detailed methods are provided in the online version of this paper and include the following:

- KEY RESOURCES TABLE
- RESOURCE AVAILABILITY
  - Lead contact
  - Materials availability
  - Data and code availability
- EXPERIMENTAL MODEL AND SUBJECT DETAILS
- METHOD DETAILS
- QUANTITATION AND STATISTICAL ANALYSIS
- ADDITIONAL RESOURCES

ACKNOWLEDGMENTS

This work was supported by National Natural Science Foundation of China (Grant Nos. 11504306, 92050102, and 11874311), Natural Science Foundation of Fujian Province (Grant Nos. 2021J01055 and 2021J01584), Fundamental Research Funds for the Central Universities (Grant Nos. 20720220134, 20720200074, and 20720220033), and China Scholarship Council (202006310049).

AUTHOR CONTRIBUTIONS

Y. Z.: Conceptualization, Software, Data curation, Writing—Original Draft, Preparation, Writing—Review & diting. Q. D.: Results Discussion, Editing. J. X.: Supervision. Z. Y.: Supervision, Editing. H. C.: Supervision, Fund support, Writing—Review & Editing. Y. L.: Conceptualization, Supervision, Fund support, Writing—Review & Editing. All authors discussed the results and commented on the article.

DECLARATION OF INTERESTS

The authors declare no conflicts of interest.

Received: November 15, 2022
Revised: January 18, 2023
Accepted: January 30, 2023
Published: February 2, 2023

REFERENCES

1. Barron, L.D. (2009). Molecular Light Scattering and Optical Activity (Cambridge University Press).

2. Papakostas, A., Potts, A., Bagnall, D.M., Prosvirnin, S.L., Coles, H.J., and Zheludev, N.I. (2003). Optical manifestations of planar chirality. Phys. Rev. Lett. *90*, 107404. https://doi.org/10.1103/PhysRevLett.90.107404.

3. Fedotov, V.A., Schwanecke, A.S., Zheludev, N.I., Khardikov, V.V., and Prosvirnin, S.L. (2007). Asymmetric transmission of light and enantiomerically sensitive plasmon resonance in planar chiral nanostructures. Nano Lett. *7*, 1996–1999. https://doi.org/10.1021/nl0707961.

4. Schwanecke, A.S., Fedotov, V.A., Khardikov, V.V., Prosvirnin, S.L., Chen, Y., and Zheludev, N.I. (2008). Nanostructured metal film with asymmetric optical transmission. Nano Lett. *8*, 2940–2943. https://doi.org/10.1021/nl801794d.

5. Singh, R., Plum, E., Menzel, C., Rockstuhl, C., Azad, A.K., Cheville, R.A., Lederer, F., Zhang, W., and Zheludev, N.I. (2009). Terahertz metamaterial with asymmetric transmission. Phys. Rev. B *80*, 153104. https://doi.org/10.1103/PhysRevB.80.153104.

6. Liu, J., Li, Z., Liu, W., Cheng, H., Chen, S., and Tian, J. (2016). High-efficiency mutual dual-band asymmetric transmission of circularly polarized waves with few-layer anisotropic metasurfaces. Adv. Opt. Mater. *4*, 2028–2034. https://doi.org/10.1002/adom.201600602.

7. Shi, J.H., Ma, H.F., Guan, C.Y., Wang, Z.P., and Cui, T.J. (2014). Broadband chirality and asymmetric transmission in ultrathin 90°-twisted Babinet-inverted metasurfaces. Phys. Rev. B *89*, 165128. https://doi.org/10.1103/PhysRevB.89.165128.

8. Tang, D.F., Wang, C., Pan, W.K., Li, M.H., and Dong, J.F. (2017). Broad dual-band asymmetric transmission of circular polarized waves in near-infrared communication band. Opt Express *25*, 11329–11339. https://doi.org/10.1364/OE.25.011329.

9. Han, B., Li, S., Li, Z., Huang, G., Tian, J., and Cao, X. (2021). Asymmetric transmission for dual-circularly and linearly polarized waves based on a chiral metasurface. Opt Express *29*, 19643–19654. https://doi.org/10.1364/OE.425787.

10. Plum, E., Fedotov, V.A., and Zheludev, N.I. (2009). Planar metamaterial with transmission and reflection that depend on the direction of incidence. Appl. Phys. Lett. *94*, 131901. https://doi.org/10.1063/1.3109780.

11. Sarkar, S., and Gupta, B. (2022). Multiband chiral metasurface for asymmetric reflection and transmission of circularly polarized waves. IEEE Antennas Wirel. Propag. Lett. *21*, 178–182. https://doi.org/10.1109/LAWP.2021.3123580.

12. Shi, J.H., Zhu, Z., Ma, H.F., Jiang, W.X., and Cui, T.J. (2012). Tunable symmetric and asymmetric resonances in an asymmetrical split-ring metamaterial. J. Appl. Phys. *112*, 073522. https://doi.org/10.1063/1.4757961.

13. Hentschel, M., Ferry, V.E., and Alivisatos, A.P. (2015). Optical rotation reversal in the optical response of chiral plasmonic nanosystems: the role of plasmon hybridization. ACS Photonics *2*, 1253–1259. https://doi.org/10.1021/acsphotonics.5b00354.

14. Cao, T., Wei, C.W., Mao, L.B., and Wang, S. (2015). Tuning of giant 2D-chiroptical response using achiral metasurface integrated with graphene. Opt Express *23*, 18620–18629. https://doi.org/10.1364/OE.23.018620.

15. Cao, T., Li, Y., Zhang, X., and Zou, Y. (2017). Theoretical study of tunable chirality from graphene integrated achiral metasurfaces. Photon. Res. *5*, 441–449. https://doi.org/10.1364/PRJ.5.000441.

16. Zhou, S., Lai, P., Dong, G., Li, P., Li, Y., Zhu, Z., Guan, C., and Shi, J. (2019). Tunable chiroptical response of graphene achiral metasurfaces in mid-infrared regime. Opt Express *27*, 15359–15367. https://doi.org/10.1364/OE.27.015359.

17. Hong, Q., Xu, W., Zhang, J., Zhu, Z., Yuan, X., and Qin, S. (2019). Optical activity in monolayer black phosphorus due to extrinsic chirality. Opt. Lett. *44*, 1774–1777. https://doi.org/10.1364/OL.44.001774.

18. Zeng, Y., Xu, J., Xiao, W., Yang, Z., Chen, H., and Liu, Y. (2022). Giant 2D-chiroptical response in an achiral metasurface integrated with black phosphorus. Opt Express *30*, 8266–8274. https://doi.org/10.1364/OE.452554.

19. Huang, Y., Yao, Z., Hu, F., Liu, C., Yu, L., Jin, Y., and Xu, X. (2017). Tunable circular polarization conversion and asymmetric transmission of planar chiral graphene-metamaterial in terahertz region. Carbon *119*, 305–313. https://doi.org/10.1016/j.carbon.2017.04.037.

20. Fedotov, V.A., Mladyonov, P.L., Prosvirnin, S.L., Rogacheva, A.V., Chen, Y., and Zheludev, N.I. (2006). Asymmetric propagation of electromagnetic waves through a planar chiral structure. Phys. Rev. Lett. *97*, 167401. https://doi.org/10.1103/PhysRevLett.97.167401.

21. Asgari, S., and Rahmanzadeh, M. (2020). Tunable circular conversion dichroism and asymmetric transmission of terahertz graphene metasurface composed of split rings. Opt Commun. *456*, 124623. https://doi.org/10.1016/j.optcom.2019.124623.

22. Plum, E., Fedotov, V.A., and Zheludev, N.I. (2011). Asymmetric transmission: a generic property of two-dimensional periodic patterns. J. Opt. *13*, 024006. https://doi.org/10.1088/2040-8978/13/2/024006.

23. Aba, T., Qu, Y., Wang, T., Chen, Y., Li, H., Wang, Y., Bai, Y., and Zhang, Z. (2018). Tunable asymmetric transmission through tilted rectangular hole arrays in a square lattice. Opt Express *26*, 1199–1205. https://doi.org/10.1364/OE.26.001199.

24. Apurv Chaitanya, N., Butt, M.A.T., Reshef, O., Boyd, R.W., Banzer, P., and De Leon, I. (2022). Lattice-plasmon induced asymmetric transmission in two-dimensional chiral arrays. APL Photonics *7*, 016105. https://doi.org/10.1063/5.0074849.

25. Shokati, E., Asgari, S., and Granpayeh, N. (2019). Dual-band polarization-sensitive graphene chiral metasurface and its application as a refractive index sensor. IEEE Sens. J. *19*, 9991–9996. https://doi.org/10.1109/JSEN.2019.2925963.

26. Masyukov, M., Vozianova, A., Grebenchukov, A., Gubaidullina, K., Zaitsev, A., and Khodzitsky, M. (2020). Optically tunable terahertz chiral metasurface based on multi-layered graphene. Sci. Rep. *10*, 3157–3210. https://doi.org/10.1038/s41598-020-60097-0.

27. Li, J., Li, J., Zheng, C., Wang, S., Li, M., Zhao, H., Li, J., Zhang, Y., and Yao, J. (2021). Dynamic control of reflective chiral terahertz metasurface with a new application developing in full grayscale near field imaging. Carbon *172*, 189–199. https://doi.org/10.1016/j.carbon.2020.09.090.

28. Amin, M., Siddiqui, O., Abutarboush, H., Farhat, M., and Ramzan, R. (2021). A THz graphene metasurface for polarization selective virus sensing. Carbon N. Y. *176*, 580–591. https://doi.org/10.1016/j.carbon.2021.02.051.

29. Cao, T., Wei, C.W., and Li, Y. (2016). Dual-band strong extrinsic 2D chirality in a highly symmetric metal-dielectric-metal achiral metasurface. Opt. Mater. Express *6*, 303–311. https://doi.org/10.1364/OME.6.000303.

30. Cao, T., Wei, C., Mao, L., and Li, Y. (2014). Extrinsic 2D chirality: giant circular conversion dichroism from a metal-dielectric-metal square array. Sci. Rep. *4*, 7442. https://doi.org/10.1038/srep07442.

31. Li, J., Li, J., Yang, Y., Li, J., Zhang, Y., Wu, L., Zhang, Z., Yang, M., Zheng, C., Li, J., et al. (2020). Metal-graphene hybrid active chiral

metasurfaces for dynamic terahertz wavefront modulation and near field imaging. Carbon *163*, 34–42. https://doi.org/10.1016/j.carbon.2020.03.019.

32. Shen, Z., and He, Q. (2021). Mutual circular polarization conversions in asymmetric transmission and reflection modes by three-layer metasurface with gold split-rings. Opt Express *29*, 34850–34862. https://doi.org/10.1364/OE.441865.

33. Rana, A.S., Kim, I., Ansari, M.A., Anwar, M.S., Saleem, M., Tauqeer, T., Danner, A., Zubair, M., Mehmood, M.Q., and Rho, J. (2020). Planar achiral metasurfaces-induced anomalous chiroptical effect of optical spin isolation. ACS Appl. Mater. Interfaces *12*, 48899–48909. https://doi.org/10.1021/acsami.0c10006.

34. Zhang, R., Zhao, Q., Wang, X., Gao, W., Li, J., and Tam, W.Y. (2019). Measuring circular phase-dichroism of chiral metasurface. Nanophotonics *8*, 909–920. https://doi.org/10.1515/nanoph-2019-0061.

35. Zhang, R., Zhao, Q., Wang, X., Li, J., and Tam, W.Y. (2020). Circular phase-dichroism of chiral metasurface using birefringent interference. Nano Lett. *20*, 2681–2687. https://doi.org/10.1021/acs.nanolett.0c00311.

36. Rodrigo, D., Limaj, O., Janner, D., Etezadi, D., García de Abajo, F.J., Pruneri, V., and Altug, H. (2015). Mid-infrared plasmonic biosensing with graphene. Science *349*, 165–168. https://www.science.org/doi/10.1126/science.aab2051.

37. Harada, Y., Ukhtary, M.S., Wang, M., Srinivasan, S.K., Hasdeo, E.H., Nugraha, A.R.T., Noe, G.T., Sakai, Y., Vajtai, R., Ajayan, P.M., et al. (2017). Giant terahertz-wave absorption by monolayer graphene in a total internal reflection geometry. ACS Photonics *4*, 121–126. https://doi.org/10.1021/acsphotonics.6b00663.

STAR★METHODS

KEY RESOURCES TABLE

REAGENT or RESOURCE	SOURCE	IDENTIFIER
Software and algorithms		
COMSOL	COMSOL China Co., LTD	http://cn.comsol.com/
MATLAB	MathWorks Co., LTD.	https://www.mathworks.com/products/matlab.html

RESOURCE AVAILABILITY

Lead contact

Further information and requests for resources and reagents should be directed to and will be fulfilled by the lead contact, Yineng Liu (lyn610@xmu.edu.cn).

Materials availability

This study did not generate new unique reagents.

Data and code availability

- Data reported in this paper will be shared by the lead contact upon request.
- This paper does not report original codes.
- Any additional information required to reanalyze the data reported in this paper is available from the lead contact upon request

EXPERIMENTAL MODEL AND SUBJECT DETAILS

The COMSOL Multiphysics software has been employed to analyze the reflection spectra and near-field patterns of the proposed graphene metasurface. In these numerical simulations, the periodic boundary conditions are set along the *x* and *y* directions and the propagation direction of incident CPW is set to be perpendicular to the *x*-*y* plane where the graphene pattern. The optical conductivity of graphene can be described by Kubo formula,[19] and the relaxation time and Fermi level of graphene are 0.64 ps and 0.9 eV, respectively.

METHOD DETAILS

The simulation is conducted with the COMSOL Multiphysics software with a frequency domain solver and tetrahedral mesh type. In the simulations, the periodic boundary conditions are set along the *x* and *y* directions. The perfectly matched layers are applied at the top and bottom of the computational domain for absorbing wave. A periodic port is applied to generate CPW and accept the reflected CPW with the same handedness, and another periodic port is applied in the same boundary to accept the reflected converted CPW. The optical conductivity of graphene can be described by Kubo formula,[19] and the relaxation time and Fermi level of graphene are 0.64 ps and 0.9 eV, respectively. The dielectric layer is set to be a lossless polyethylene cyclic olefin copolymer with a permittivity of 2.35. The metal substrate is modeled as a dispersive silver using Drude model: $\varepsilon_m = \varepsilon_\infty - \omega_p^2/(\omega^2 + i\omega\gamma)$. Here, ω is the angular frequency, and $\omega_p = 1.39 \times 10^{16}$ rad/s is the plasma frequency, $\gamma = 2.7 \times 10^{13}$ rad/s is the scattering rate, and $\varepsilon_\infty = 3.4$ is the high-frequency constant.

QUANTITATION AND STATISTICAL ANALYSIS

The simulation data is produced by COMSOL Multiphysics software. Figures shown in the main text were produced by MATLAB and Microsoft PowerPoint from the raw data.

ADDITIONAL RESOURCES

Any additional information about the simulation and data reported in this paper is available from the lead contact on request.